

## 3-D Modeling of a composite material reinforced with multiple thickly coated particles using the infinite element method

D.S. Liu<sup>1,2</sup>, C.Y. Chen<sup>2</sup>, D.Y. Chiou<sup>3</sup>

**Abstract:** A three-dimensional heterogeneous infinite element method (HIEM) for modeling inclusions with interphases in composite materials is presented. This special element is formulated based on the conventional finite element method (FEM) using the similarity stiffness property and matrix condensation operations. An HIE-FE coupling scheme is also developed and implemented using the commercial software *ABAQUS* to conduct the elastostatic analysis. The proposed approach was validated first to study heterogeneous material containing one spherical inclusion. The displacement and stress variations around the inclusion vicinity are verified against conventional FEM. The proposed approach was next applied to analyze the effective modulus of single-particle and  $2 \times 2 \times 2$ -particles cubic models with the presence of interphases. The effects of varying the modulus and thickness of the interphase are also examined. The influences of multiple inclusion orientation arrangements are investigated. The results show that different model orientation arrangements can have marked influences on the effective elastic modulus evaluation for particulate-reinforced composites.

**keyword:** Particulate-reinforced composites, Heterogeneous material, Infinite element method, Modeling multiple particles.

### 1 Introduction

One of the main engineering problems is predicting the mechanical behaviors of heterogeneous materials (ex. particulate-reinforced and fiber-reinforced composites),

in which the constituent material properties are different and heterogeneous. Many researchers have expended great effort to develop various modeling and calculation techniques involving heterogeneous materials with inclusions.

Zhang and Katsube (1995) proposed a hybrid finite element approach for the mechanical analysis of heterogeneous materials with randomly dispersed inclusions or voids. In this method an n-sided polygonal super-element containing an inclusion was developed from a modified hybrid functional based on the Hellinger-Reissner principle. In the element formulation, classical elasticity solutions were required to incorporate the approximating functions. Using these functions the irregular stress and displacement distributions around the inclusion could be well represented. However, different hybrid functions are required for the matrix and inclusion, respectively. The analytical approach for complex inclusion geometry usually results in difficult mathematical calculations, making the classical elasticity solutions not easily available. Furthermore, no works have attempted to model the interphases that play important roles in the overall mechanical behavior of composite materials.

The boundary element method (BEM) has also been applied to the micro-mechanical behaviors of composite materials with thin films or coatings [Luo, Liu and Berger (1998), Luo, Liu and Berger (2000), Liu, Xu and Luo (2000), Chen and Liu (2001)]. Recently, Okada, Fukui and Kumazawa (2004) successfully modeled the distributed particles by using the analytical solutions for ellipsoidal particles and obtained the effective mechanical properties of particulate composite materials having up to 1000 particles. However, to derive the BEM boundary integral equation formulation, a fundamental solution function that satisfies the governing differential equation in the domain is required as a basic function for an approximate solution. Furthermore, numerous numerical integrations must be performed and the subsequent

<sup>1</sup> Corresponding author. Tel.: +886-5-2720411 (Ext: 33305); fax.: +886-5-2720589, imedsl@ccu.edu.tw

<sup>2</sup> Department of Mechanical Engineering, National Chung Cheng University, 160, San-Hsing, Ming-Hsiung, Chia-Yi, 621, Taiwan, ROC

<sup>3</sup> Industrial Technology Research Institute (CAST/ITRI), Rm. 130, Bldg. 52, 195 Sec. 4, Chung Hsing Road Chutung, Hsinchu 310, Taiwan, ROC

global coefficient matrix formed from BEM is usually fully populated and non-symmetrical, leading to increasing direct solution computational expense for the coefficient matrix.

The conventional finite element method (FEM) has been used to solve the mechanical behaviors of fiber-reinforced composites [Lagache, Agbossou, Pastor and Muller (1994), Wacker, Bledzki and Chate (1998)] and particulate-reinforced composites [Agrwal and Broutman (1974), Wu and Dong (1995)] with interphases. A three-dimensional multi-inclusion unit cell with randomly positioned and oriented particles was developed by Böhm, Han and Eckschlager (2004). However, the corresponding CPU time and PC memory storage requirement is huge for an accurate mechanical field solution. Moreover, for problems with interphases, a thin layer of very fine finite elements is used to model the interphase between the inclusion and matrix. With the decrease in interphase thickness, a large number of elements are needed to avoid element mesh with the large aspect ratio. This may cause deteriorated FE solutions with excessive prohibitive investment in terms of the computational cost and analytical effort. To avoid the difficulty of building a FE model for particulate composite material, an element overlay technique has been developed to investigate the problems of samples containing many distributed voids and filled particles [Okada, Liu, Ninomiya, Fukui and Kumazawa (2004)]. However, the solutions are very sensitive to the size of the local element (the element contained particle), and a large number of integration points are used demanding a considerable amount of computational time.

Liu and Chiou (2003) recently focused their attention on the developments of 2-D and 3-D infinite element method (IEM). The IEM approach was implemented into computer codes to deal with various types of classical elasticity and singularity problems. The related background and information on this matter are summarized in [Silvester and Cermak (1969), Thatcher (1975), Thatcher (1978), Guo (1979), Ying (1995)].

The IEM analysis is limited to cases in which the constituent material properties of the medium in the IE sub-domain are assumed homogeneous. Therefore, a heterogeneous infinite element method for modeling two-dimensional heterogeneous materials is developed [Liu and Chiou (2005)].

In this study the heterogeneous infinite element method

is extended to deal with three-dimensional elastostatic problems in which the constituent material properties are heterogeneous. For that reason, modeling three-dimensional heterogeneous composite material reinforced with multiple thickly coated particles is our interest. A numerical example is evaluated first to predict the displacement and stress variation around the imbedded inclusions. The proposed method is also verified against finite element solutions. Both single particle and  $2 \times 2 \times 2$  particle models containing inclusions with the surrounding interphase are considered. The effects of varying interphase modulus and thickness in determining the effective Young's modulus are investigated. The orientation arrangement effects of the inclusions on the effective Young's modulus are then discussed. Our conclusions are given last.

## 2 3-D heterogeneous infinite element method (HIEM) formulation

The heterogeneous infinite element method (HIEM) formulation for 3-D elastostatic problems is presented in this section. Let us consider a special element in which an elastic inclusion or a void of arbitrary geometry exists (in this section, the geometry is hexahedral), as shown in Fig. 1(a). Our objective is to establish the relationship between the element's nodal forces and displacements, to formulate the element stiffness matrix. As shown in Figs. 1(b) and (c), the domain over the special element is decomposed into two sub-domains with different material characteristics, which represent: (i) the interphase sub-domain with boundaries  $\Gamma_0$  and  $\Gamma_s$ ; (ii) the inclusion sub-domain with boundary  $\Gamma_s$ .  $\Gamma_0$  and  $\Gamma_s$ , are the element's outer boundary with neighboring elements and the inner interface boundary between the interphase and inclusion sub-domains. In the following formulation, the material properties are assumed linearly elastic, isotropic, but heterogeneous from individual sub-domains. The separate formulations for these two sub-domains are derived (index notation is used here) as follows:

### 2.1 Formulation in the interphase sub-domain

The similar partition concept [Guo (1979)] is applied to the interphase region shown in Fig. 2. First, the primary domain boundary surface,  $\Gamma_0$ , is properly distributed using a number of  $n$  master nodes and discretized into virtual eight-node hexahedral elements. Second, by choosing the global origin  $O$  located in the inclusion region,

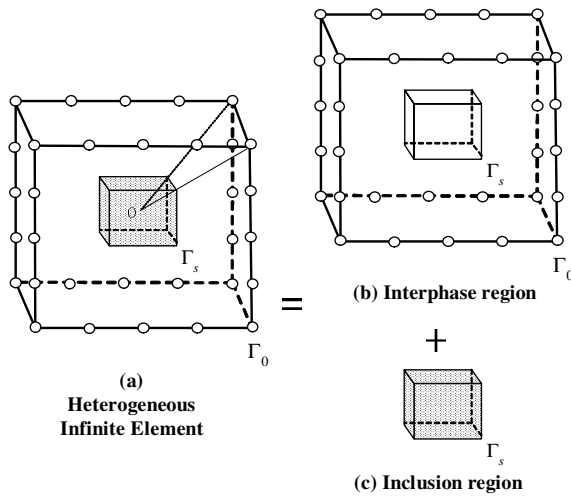


**Figure 1** : Element decomposition: (a) original heterogeneous infinite element; (b) interphase region; (c) inclusion region

as a similar partition center, and taking a certain number of chosen element-layers  $s$  and a certain proportionality constant  $k \in (0, 1)$  which are compatible, similar surfaces  $\Gamma_1, \Gamma_2, \dots, \Gamma_s$ , of  $\Gamma_0$  are constructed with center  $O$  according to the proportionality constants  $k^1, k^2, \dots, k^s$ , respectively. The region bounded between  $\Gamma_{i-1}$  and  $\Gamma_i$  is called the  $i$ -th element-layer ( $i = 1, 2, \dots, s$ ), where  $s$  is the number of chosen element-layers. Third, each individual  $\Gamma_i$  is regularly discretized as  $\Gamma_0$ . The nodal number and node coordinates on each individual  $\Gamma_i$  can be determined from the master node coordinates with geometrically similar conditions. Fourth, every element-layer is auto-meshed into eight-node hexahedral elements that are similar to one another in a radial direction.

When the first element-layer is considered, the element stiffness matrix of each hexahedral element can be calculated and assembled into an element-layer stiffness matrix using the conventional FE formulation. The stiffness matrix of the “first element-layer” can be calculated and expressed as

$$\begin{bmatrix} K_a & -A^T \\ -A & K_b \end{bmatrix}_{6m \times 6m} \quad (1)$$

where  $K_a, K_b$ , and  $A$  are the sub-matrices of the stiffness matrix with identical dimension  $3m \times 3m$ .  $A^T$  is the transpose of  $A$ . The nodal displacement vector  $\delta_i$  of the nodes of  $\Gamma_i$  is defined as

$$\delta_i \equiv [u_1^i \ v_1^i \ w_1^i \ \dots \ u_m^i \ v_m^i \ w_m^i]^T \quad (2)$$

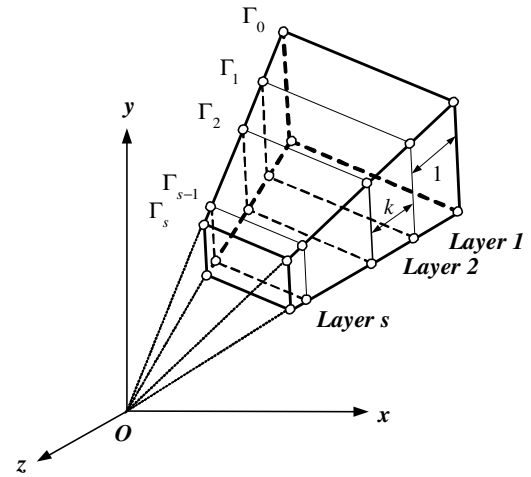


**Figure 2** : Infinite element mesh for the interphase region

The nodal force vector  $f_i$  of nodes on  $\Gamma_i$  is defined as

$$f_i \equiv [f_{1x}^i \ f_{1y}^i \ f_{1z}^i \ \dots \ f_{mx}^i \ f_{my}^i \ f_{mz}^i]^T \quad (3)$$

The  $i$ -th element-layer stiffness matrix presents the nodal force and displacement vector relationships between  $\Gamma_{i-1}$  and  $\Gamma_i$ . Treating the first element-layer as an example, we have

$$\begin{bmatrix} K_a & -A^T \\ -A & K_b \end{bmatrix} \cdot \begin{bmatrix} \delta_0 \\ \delta_1 \end{bmatrix} = \begin{bmatrix} f_0 \\ f_1 \end{bmatrix} \quad (4)$$

Two algebraic equations are extracted from Eq. 4 as following

$$K_a \delta_0 - A^T \delta_1 = f_0 \quad (5)$$

$$-A \delta_0 + K_b \delta_1 = f_1 \quad (6)$$

where  $\delta_0$  and  $f_0$ , denote the nodal displacements and tractions on  $\Gamma_0$ , respectively. According to the similarity principle, it is obvious that the stiffness matrices of all of the element-layers are directly proportional to the element size. Hence, we can express the stiffness matrices of the  $s$  element-layers (from 1st element-layer to  $s$ -th element-layer) as  $s$  sets of algebraic equations, namely

for layer 1

$$\begin{bmatrix} K_a & -A^T \\ -A & K_b \end{bmatrix} \cdot \begin{bmatrix} \delta_0 \\ \delta_1 \end{bmatrix} = \begin{bmatrix} f_0 \\ f_1 \end{bmatrix} \quad (7)$$

for layer 2

$$k \cdot \begin{bmatrix} K_a & -A^T \\ -A & K_b \end{bmatrix} \cdot \begin{bmatrix} \delta_1 \\ \delta_2 \end{bmatrix} = \begin{bmatrix} -f_1 \\ f_2 \end{bmatrix} \quad (8)$$

for layer 3

$$k^2 \cdot \begin{bmatrix} K_a & -A^T \\ -A & K_b \end{bmatrix} \cdot \begin{bmatrix} \delta_2 \\ \delta_3 \end{bmatrix} = \begin{bmatrix} -f_2 \\ f_3 \end{bmatrix} \quad (9)$$

⋮

for layer s

$$k^{s-1} \cdot \begin{bmatrix} K_a & -A^T \\ -A & K_b \end{bmatrix} \cdot \begin{bmatrix} \delta_{s-1} \\ \delta_s \end{bmatrix} = \begin{bmatrix} -f_{s-1} \\ f_s \end{bmatrix} \quad (10)$$

Extracting with every algebraic equation, adding the second equation for the i-th element-layer and the first equation for the (i+1)-th element-layer, and letting  $P = kK_a + K_b$ , we have

$$K_a \delta_0 - A^T \delta_1 = f_0 \quad (11)$$

$$-A \delta_0 + P \delta_1 - kA^T \delta_2 = 0 \quad (12)$$

⋮

$$-k^{i-1} A \delta_{i-1} + k^{i-1} P \delta_i - k^i A^T \delta_{i+1} = 0 \quad (13)$$

⋮

$$-k^{s-2} A \delta_{s-2} + k^{s-2} P \delta_{s-1} - k^{s-1} A^T \delta_s = 0 \quad (14)$$

$$-k^{s-1} A \delta_{s-1} + k^{s-1} K_b \delta_s = f_s \equiv F_s \quad (15)$$

## 2.2 Formulation in the inclusion sub-domain

The partition processes for the inclusion region, shown in Fig. 3, are followed in a manner similar to that for the interphase region. The inner boundary  $\Gamma_s$  of the interphase region is exactly the outer boundary of the inclusion region. By choosing the global origin O as the similar partition center and taking another proportionality constant  $\rho$  and element-layer p, similar surfaces  $\Gamma_{s+1}$ ,  $\Gamma_{s+2}$ ,  $\dots$ ,  $\Gamma_{s+p}$  of  $\Gamma_s$  are generated with center O according to the proportionality constants  $\rho^1$ ,  $\rho^2$ ,  $\dots$ ,  $\rho^p$ , respectively. The region bounded between  $\Gamma_{j-1}$  and  $\Gamma_j$  is called the j-th element-layer ( $j = s+1, s+2, \dots, s+p$ ).

We also express the stiffness matrix of the p element-layers (from (s+1)-th element-layer to (s+p)-th element-layer) as s sets of algebraic equations, namely

for layer s + 1

$$\begin{bmatrix} K_c & -B^T \\ -B & K_d \end{bmatrix} \cdot \begin{bmatrix} \delta_s \\ \delta_{s+1} \end{bmatrix} = \begin{bmatrix} -f_s \\ f_{s+1} \end{bmatrix} \quad (16)$$

for layer s + 2

$$\rho \cdot \begin{bmatrix} K_c & -B^T \\ -B & K_d \end{bmatrix} \cdot \begin{bmatrix} \delta_{s+1} \\ \delta_{s+2} \end{bmatrix} = \begin{bmatrix} -f_{s+1} \\ f_{s+2} \end{bmatrix} \quad (17)$$

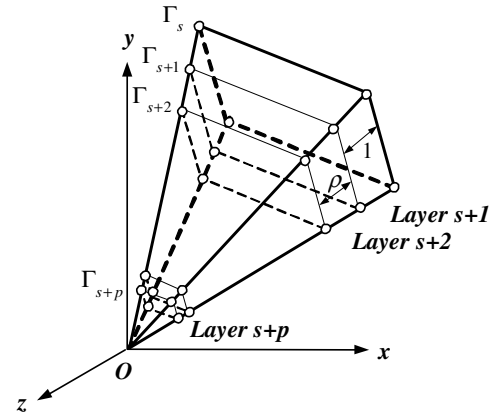


**Figure 3** : Infinite element mesh for the inclusion region

for layer s + 3

$$\rho^2 \cdot \begin{bmatrix} K_c & -B^T \\ -B & K_d \end{bmatrix} \cdot \begin{bmatrix} \delta_{s+2} \\ \delta_{s+3} \end{bmatrix} = \begin{bmatrix} -f_{s+2} \\ f_{s+3} \end{bmatrix} \quad (18)$$

⋮

for layer s + p

$$\rho^{p-1} \cdot \begin{bmatrix} K_c & -B^T \\ -B & K_d \end{bmatrix} \cdot \begin{bmatrix} \delta_{s+p-1} \\ \delta_{s+p} \end{bmatrix} = \begin{bmatrix} -f_{s+p-1} \\ f_{s+p} \end{bmatrix} \quad (19)$$

Extracting every algebraic equation, adding the second equation for the j-th element-layer and the first equation for the (j+1)-th element-layer, and letting  $Q = \rho K_c + K_d$ , we have

$$K_c \delta_s - B^T \delta_{s+1} = -f_s \quad (20)$$

$$-B \delta_s + Q \delta_{s+1} - \rho B^T \delta_{s+2} = 0 \quad (21)$$

⋮

$$-\rho^{j-(s+1)} B \delta_{j-1} + \rho^{j-(s+1)} Q \delta_j - \rho^{j-s} B^T \delta_{j+1} = 0 \quad (22)$$

⋮

$$-\rho^{p-2} B \delta_{s+p-2} + \rho^{p-2} Q \delta_{s+p-1} - \rho^{p-1} B^T \delta_{s+p} = 0 \quad (23)$$

$$-\rho^{p-1} B \delta_{s+p-1} + \rho^{p-1} K_d \delta_{s+p} = f_{s+p} \equiv F_{s+p} \quad (24)$$

Let  $M_{s+p} = K_d$  and  $F_{s+p} = f_{s+p}$ , the three IEM parameters in iteration form representing for the inclusion region can be inferred:

$$M_i = Q - \rho B^T M_{i+1}^{-1} B \quad (25)$$

$$F_i = B^T M_{i+1}^{-1} F_{i+1} \quad (26)$$

$$\delta_j = \rho^{-(j-(s+1))} M_j^{-1} \left( \rho^{(j-(s+1))} B \delta_{j-1} + F_j \right) \quad (27)$$

where  $i = s+1, s+2, s+3, \dots, s+p-1$ ; and  $j = s+1, s+2, s+3, \dots, s+p$ .

From Eq. 27, we have

$$\delta_{s+1} = M_{s+1}^{-1} (B \delta_s + F_{s+1}) \quad (28)$$

By substituting Eq. 28 into Eq. 20, we get

$$K_c \delta_s - B^T [M_{s+1}^{-1} (B \delta_s + F_{s+1})] = -f_s \quad (29)$$

Rearrange Eq. 29 and we have

$$(K_c - B^T M_{s+1}^{-1} B) \delta_s = [B^T M_{s+1}^{-1} F_{s+1} + (-f_s)] \quad (30)$$

Eq. 30 can be expressed in concise form as

$$K_{(inclusion)} \delta_s = F_{(inclusion)} \quad (31)$$

where  $K_{(inclusion)}$  and  $F_{(inclusion)}$  denote the combined stiffness matrix and associated loading vector for the inclusion region, respectively. Along the inclusion/interphase interface  $\Gamma_s$ ; however, the displacement compatibility and force equilibrium must be satisfied. Therefore, the Eqs. 15 and 31 are combined and we have

$$\begin{aligned} & -k^{s-1} A \delta_{s-1} + (k^{s-1} K_b + K_{(inclusion)}) \delta_s \\ & = B^T M_{s+1}^{-1} F_{s+1} \equiv F_{s(modified)} \end{aligned} \quad (32)$$

Eq. 32 can be expressed as another form

$$-k^{s-1} A \delta_{s-1} + k^{s-1} K_{b(modified)} \delta_s = F_{s(modified)} \quad (33)$$

Again, letting  $M_s = K_{b(modified)}$  and  $F_s = F_{s(modified)}$ , the three IEM parameters in iteration form representing for the interphase region can be inferred as follows:

$$M_i = P - k A^T M_{i+1}^{-1} A \quad (34)$$

$$F_i = A^T M_{i+1}^{-1} F_{i+1} \quad (35)$$

$$\delta_j = k^{-(j-1)} M_j^{-1} (k^{j-1} A \delta_{j-1} + F_j) \quad (36)$$

where  $i = 1, 2, 3, \dots, s-1$ ; and  $j = 1, 2, 3, \dots, s$ .

Since  $M_s$  and  $F_s$  are known, then  $M_{s-1}, M_{s-2}, \dots, M_1$ ;  $F_{s-1}, F_{s-2}, \dots, F_1$  can be iterated using Eqs. 34 and 35, respectively. From Eq. 36, we have  $\delta_1 = M_1^{-1} (A \delta_0 + F_1)$ .

Substituting  $\delta_1$  into Eq. 11, we obtain the most important formula for 3-D HIEM. That is

$$(K_a - A^T M_1^{-1} A) \cdot \delta_0 = (A^T M_1^{-1} F_1 + f_0) \quad (37)$$

Eq. 37 can be expressed in concise form as

$$K_Z \delta_0 = F_Z \quad (38)$$

Where  $K_Z$  and  $F_Z$  denote the combined element stiffness matrix and associated combined loading vector, respectively. Once  $F_Z$  is determined,  $\delta_0$  can be obtained from Eq. 38. Then  $\delta_1, \delta_2, \dots, \delta_s, \delta_{s+1}, \dots$ , and  $\delta_{s+p}$  can be obtained sequentially from Eqs. 36 and 27.

Comparing Eq. 38 with the results from the previous work [Liu and Chiou (2003)], we obtain parallel statements for the homogeneous and heterogeneous IEM representation. The combined element stiffness matrix  $K_Z$  term preserves the effects of involving material heterogeneity. The combined loading vector  $F_Z$  term contains both the outer and inner surface traction effects. With the HIEM, only master nodes on the boundary need to be defined. All of the inner-layer elements and nodes are condensed and transformed into only one combined element with master nodes along outer boundary  $\Gamma_0$  only. This is called the ‘‘Heterogeneous Infinite Element (HIE)’’, as schematically shown in Fig. 4. It can be viewed as a process of element elimination. The inner elements and nodes seem ‘‘imaginary and virtual’’, but they ‘‘really’’ exist and work in HIEM manipulations.

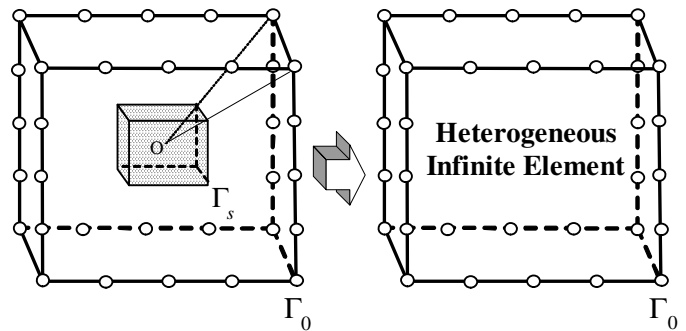


**Figure 4** : Schematic diagram of Heterogeneous Infinite Element formation

From the physical point of view, the  $K_Z$  term can be treated as the equivalent stiffness matrix of the HIE with a dimension of  $3m \times 3m$ . Although the total degree of freedom of  $K_Z$  is largely reduced, the mesh refinement and material heterogeneity effect are maintained

and does not increase any corresponding round-off errors because of the specific matrix condensation process. The corresponding PC memory storage requirement is also significantly reduced. Moreover, to compute  $K_Z$ , only to calculate the first element-layer stiffness matrix in the interphase and inclusion regions with the chosen proportionality constants  $k$  and  $\rho$  and the number of element-layer  $s$  and  $p$  are required.

### 3 Integration of HIE-FE coupling scheme with commercial FEM software

Following the identical pattern to the IE-FE coupling scheme [Liu and Chiou (2003)], the HIE-FE coupling scheme is also developed. Fig. 5 schematically shows the coupling scheme in which a global model is partitioned into two domains,  $\Omega$  and  $D$ , modeled using the HIE and FE, respectively. Furthermore, the HIE-FE coupling scheme used in this study is carried out using the commercial FEM software *ABAQUS/Standard*.

All related HIEM numerical procedures were programmed and executed in the *MATLAB v.5.3* language [Kwon and Bang (2000)]. After the HIEM mathematical manipulations, the special element we call “Heterogeneous Infinite Element (HIE)” is generated (see Section 2). The HIE is regarded as a regular finite element and its element properties are obtained from the pre-determined HIE stiffness matrix  $K_Z$ . The HIE definition is not included in the *ABAQUS* element library; therefore, the HIE is designated as a “user-defined element” that represents a geometric part of the model. In the *ABAQUS* codes, the user-defined elements are introduced using the \*USER ELEMENT option. In general cases a linear user-defined element can be defined as a stiffness matrix. The stiffness matrix can be distilled from the *Matlab* results ( $K_Z$ ) and defined using the \*MATRIX option. The numerical property values associated with the linear user-defined elements are defined using the \*UEL PROPERTY option and, optionally, the \*MATRIX option. For further details on this implementation, please refer to the *ABAQUS* user’s manual [Hibbitt, Karlsson and Sorensen (2002)].

### 4 Validation of the 3-D HIE-FE model

Fig. 6 shows the HIE-FE computational model with one three-dimensional elastic cube inclusion with thickness, width, and height dimensions (120 mm×120 mm×120

mm). where  $D$  represents the HIE sub-domain, and  $\Omega$  represents the FE sub-domain. Uniform tensile stress,  $\sigma_0 = 100 \text{ N/mm}^2$ , are applied to the cube. The material properties of the cube and the inclusion are: Young’s modulus  $E_m = 10^5 \text{ N/mm}^2$  and  $E_p = 10^3 \text{ N/mm}^2$ , respectively.

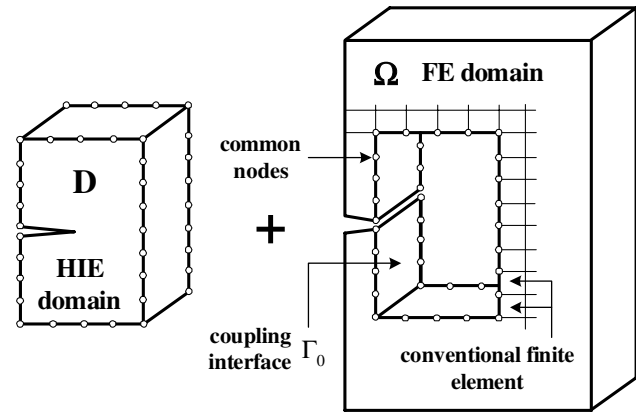


**Figure 5** : Schematic diagram of HIE-FE coupling method

In the HIE-FE model, the cube is partitioned into 1008 conventional eight-node solid elements as in the FE sub-domain (matrix region) and one 194-node heterogeneous infinite element (radius = 50 mm) with an inclusion as in the HIE sub-domain, respectively. The HIE sub-domain contains the spherical inclusion (inclusion region) and its surrounding material (interphase region). In this case, the material properties defined in the interphase region are identical to those in the matrix region, so that no interphase is modeled and perfect bonding between the inclusion and the block is assumed. Here, the main function of the interphase region is to accurately capture the irregular stress distribution close to the inclusions.

The corresponding HIEM parameters for the inclusion and interphase regions are: proportionality constant  $\lambda_p = 0.8$  and  $\lambda_m = 0.9726549474$ ; and number of element-layers  $s_p = 50$  and  $s_m = 50$ . After HIEM formulation the HIE stiffness matrix is calculated and assembled into the global stiffness matrix formed in FE sub-domain. An HIE and conventional FEM combination is established through the commercial software *ABAQUS/Standard*.

To compare the validity and performance of our proposed HIEM, FEM is used to determine the displacement and stress in the interphase region. Because we want to capture the displacement and stress variation around vicinity

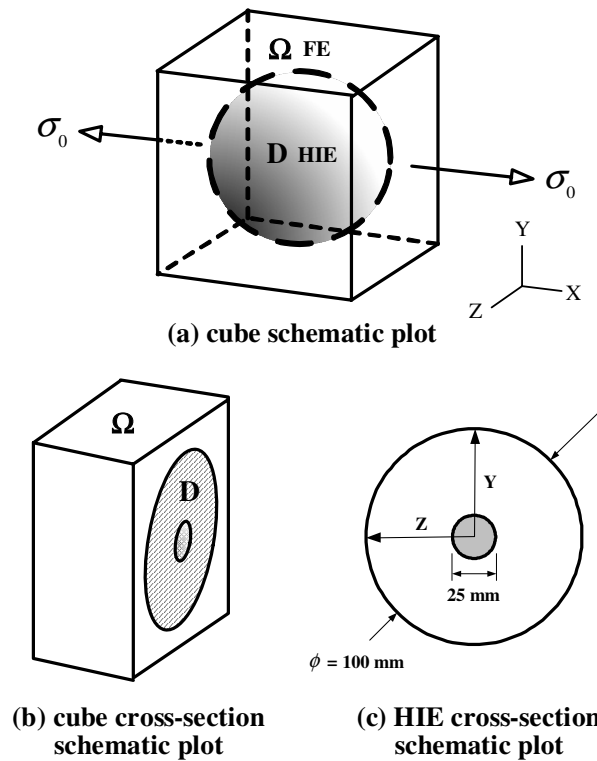


**Figure 6** : A cube with a small inclusion under uniform tensile stress used HIE-FE computational model: (a) cube schematic plot; (b) cube cross-section schematic plot; (c) HIE cross-section schematic plot

of the inclusion well, FEM have to use more elements and nodes in the interphase region as Fig. 7 (b). Fig. 7 (a) shows the less nodes and elements are needed in the HIE-FE computational mode.

The graphs comparing the nodal displacement fields along x, y, and z axis obtained from the FEM and the present HIE solution are shown in Figs. 8-10, respectively. The results are shown to be in very good agreement.

Fig. 11-13 show the normalized stresses along x, y, and z axis in the interphase region. It can be observed that our proposed HIEM results have some difference from FEM, but the solution trend is the same. It is because that HIEM obtains the node stress values from gauss integral points using the average, which is different from the commercial FEM software. The solution curves produced using our proposed HIEM are smoother than that produced using FEM, namely the stress variation around the inclusion vicinity is well captured using the proposed method.

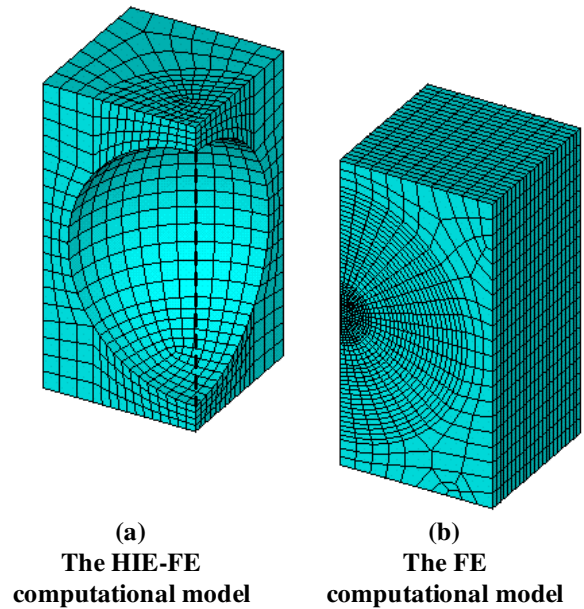


**Figure 7** : Three-dimensional 1/4 model: (a) The HIE-FE computational model; (b) The FE computational model

These figures clearly show that the displacements and stresses predicted from the proposed method are shown to be in good agreement with produced by the finite element method. The results imply that the proposed specially formulated element can be used for representing any heterogeneous material including either porous materials or materials with rigid inclusions.

### 5 The effective Young's modulus for composite material

Our proposed HIEM is applied to model 3-D composite material reinforced with multiple thickly coated particles (inclusions). For study convenience the constituents are assumed to be isotropic. Perfect bonding is assumed at the interfaces between particle and interphase and between interphase and matrix. Spherical inclusions are assumed to be packed a cube.

The effect of varying interphase material properties on determining the effective Young's modulus of the thickly coated particle composite is studied. In Fig. 14, the effective Young's modulus in the x-direction is determined by

$$\tilde{E} = \frac{\bar{\sigma}}{\bar{\epsilon}} = \frac{\bar{\sigma}}{\delta/L} \tag{39}$$

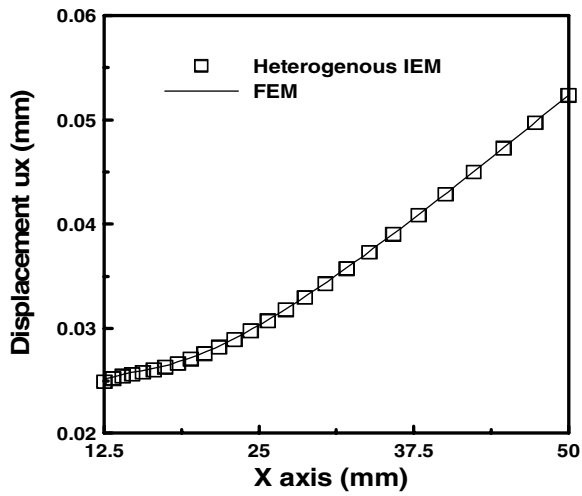


Figure 8 : Displacement along x axis

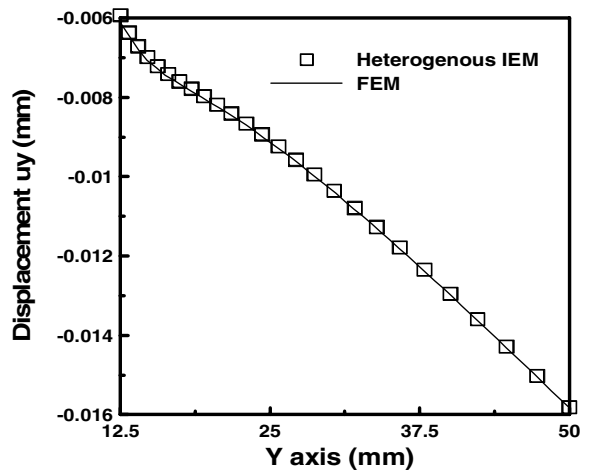


Figure 9 : Displacement along y axis

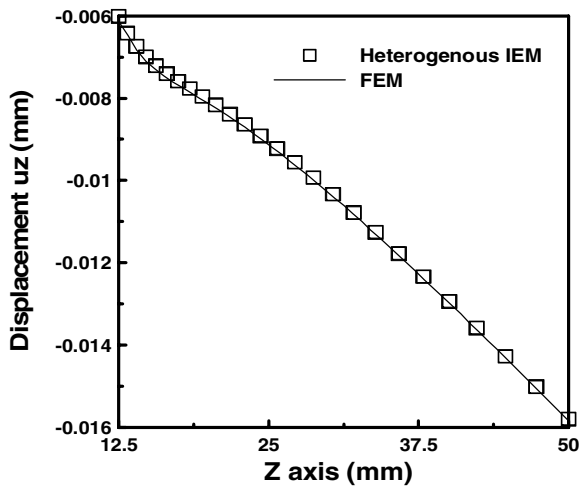


Figure 10 : Displacement along z axis

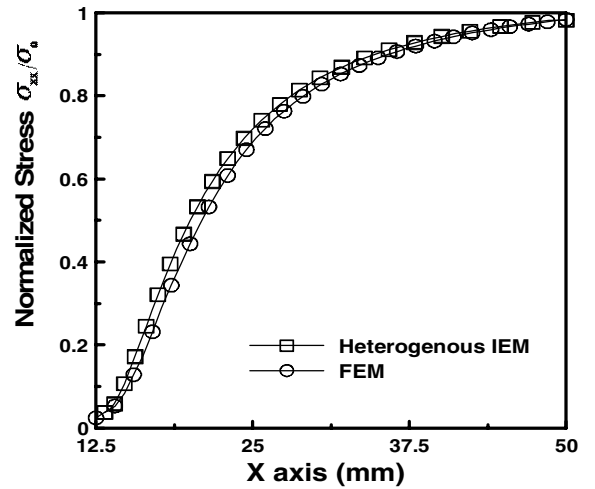


Figure 11 : Normalized stress along x axis

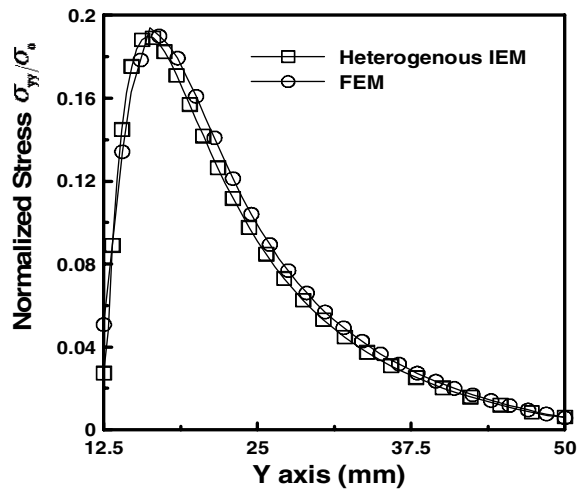


Figure 12 : Normalized stress along y axis

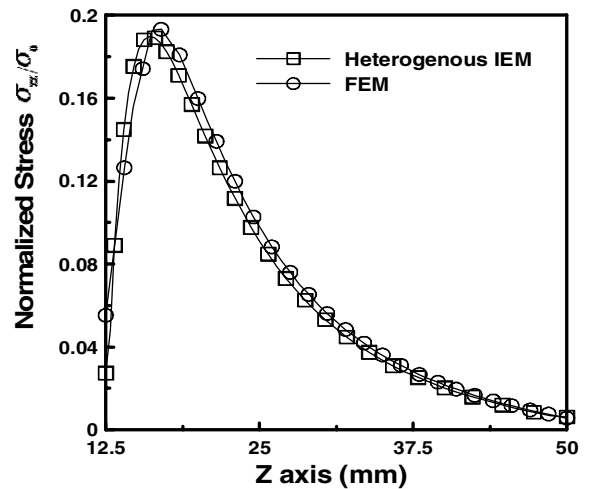
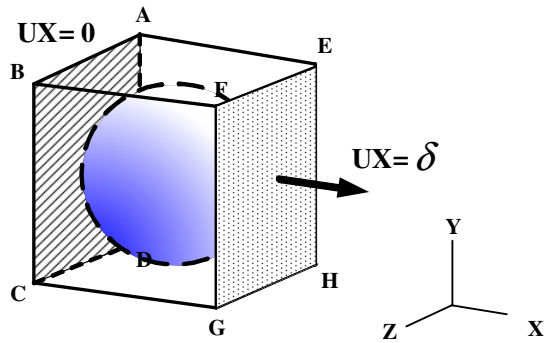
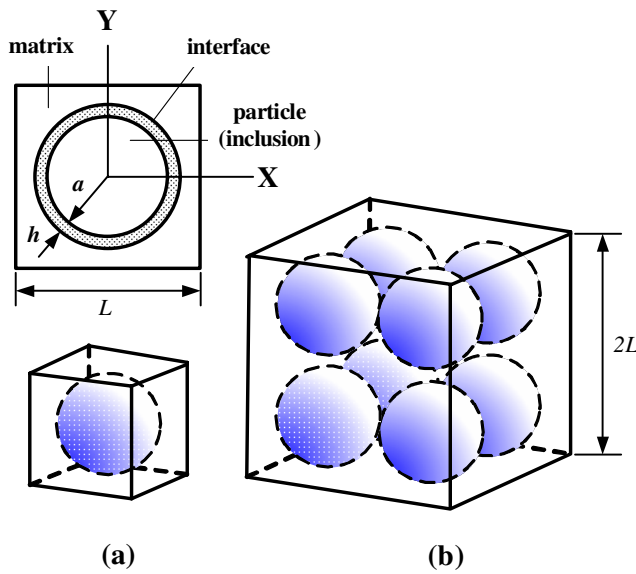


Figure 13 : Normalized stress along z axis



**Figure 14 :** Cubic single particle model under a uniform stretch



**Figure 15 :** Cubic models with thickly coated particles (inclusions): (a) single particle model; (b)  $2 \times 2 \times 2$  particles model

where  $\bar{\epsilon} = \delta/L$  is the strain in the x-direction. The stress  $\bar{\sigma}$  is calculated as

$$\bar{\sigma} = \frac{\int_A \sigma dA}{A} = \frac{1}{A} \sum_{i=1}^n \sigma A_i \quad (40)$$

where  $\sigma$  is the stress in an element and  $A_i$  is the area of the element on the face EFGH and  $n$  is the total number of such elements.

### 5.1 Influences of the Young's modulus on interfaces

Two types of cubic models are illustrated in this section, namely the single particle model and the  $2 \times 2 \times 2$  particles model both of which include the thickly coated (interphase), as shown in Fig. 15 (a) and (b). The  $2 \times 2 \times 2$

particles HIE-FE model is composed of eight the single particle model.

The cubic single particle model is first subjected a unit stretch  $\delta$  in the x-direction as shown in Fig. 14. A spherical particle (inclusion) of radius  $a$ , surrounded with a thin coating (interphase) having a uniform thickness  $h$ , is embedded within the cubic model (matrix) with length  $L$ . The dimensions are:  $a = 8.5 \mu m$ ,  $h = 1 \mu m$ , and  $L = 21.31 \mu m$ . The properties of the constituent materials considered are listed in Tab. 1. The interphase Young's modulus is a changing in the range between 4.0 and 12.0 GPa. The IEM parameters of the inclusion and interphase regions, respectively, are:  $\lambda_{in} = 0.8$  and  $\lambda_m = 0.9889390635$ ;  $s_{in} = 50$  and  $s_m = 10$ . In the single particle HIE-FE model, a total of 362 master nodes are used to simultaneously model the inclusion and interphase regions in the HIE sub-domain, and 1680 eight-node solid elements in the FE sub-domain.

As Fig. 15 (b), in the  $2 \times 2 \times 2$  particles HIE-FE model which is composed of eight the same the single particle model, a total of 2896 master nodes are used with 362 ones on each of the eight HIE sub-domains, and 13488 eight-node solid elements in the FE sub-domain. Only one inclusion with its HIE stiffness matrix needs to be calculated for the others.

Tab. 2 shows the effective Young's modulus obtained using the single particle model and the  $2 \times 2 \times 2$  particles model. It is clearly shown in Fig. 16 that subsequently increasing the interface Young's modulus and the number of inclusions involved in the model would lead to increasing the effective Young's modulus.

**Table 1 :** The properties of the constituent materials for the cubic model

Constituent Materials	Young's Modulus (GPa)	Poisson's ratio
Particle (inclusion)	$E(p) = 84.0$	$\nu(p) = 0.22$
Coating (inter-phase)	$E(in) = 4.0 \sim 12.0$	$\nu(in) = 0.34$
Matrix	$E(m) = 4.0$	$\nu(m) = 0.34$

### 5.2 Influences of the thickness on interphase

In the previous section, the interphase thickness is considered as a constant value of  $h = 1 \mu m$ . Next, the effect of varying interphase thickness on determining the effective Young's modulus is investigated. The thickness for

**Table 2** : Results of the effective Young’s modulus  $E_x$  (GPa) for different interphase Young’s modulus in the two types of cubic models

Interphase Property $E(in)$ (GPa)	4.0	6.0	8.0	12.0
Model 1. (single)	6.5725	7.0755	7.3885	7.7611
Model 2. ( $2 \times 2 \times 2$ )	6.8019	7.3486	7.6879	8.0905

**Table 3** : Results of the effective Young’s modulus  $E_x$  (GPa) for different interphase thickness in the two types of cubic models

Interphase Thickness $h(\mu m)$	1.0	0.7	0.5	0.2
Model 1. (single)	7.0755	7.0046	6.9732	6.9108
Model 2. ( $2 \times 2 \times 2$ )	7.3486	7.2642	7.2360	7.1609

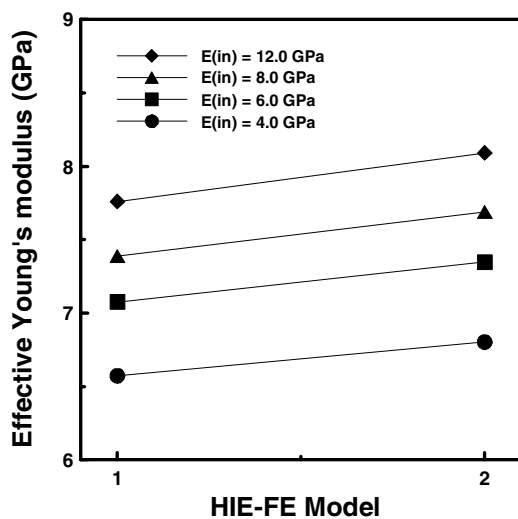


**Figure 16** : The Influences of interface Young’s modulus on the effective Young’s modulus

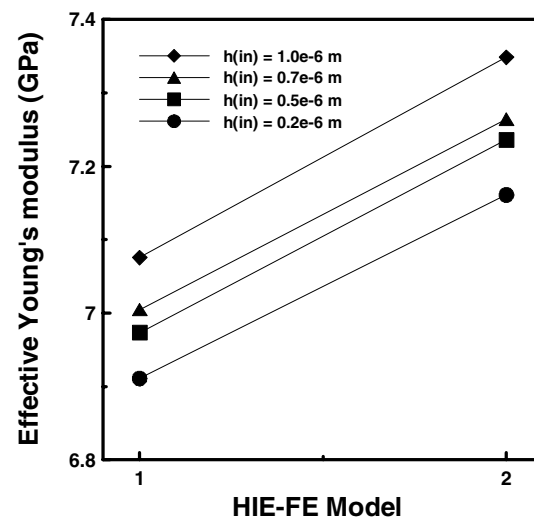


**Figure 17** : The Influences of interface thickness on the effective Young’s modulus

the interphase is changing in the range from 1.0 to 0.2 $\mu m$ . Identical constituent material constants as listed in previous section are used except the interphase Young’s modulus is considered  $E(in) = 6.0$  GPa.

Tab. 3 shows the effect of different interphase thicknesses on the effective Young’s modulus for the single particle model and the  $2 \times 2 \times 2$  particles model. The thickness influence on the effective Young’s modulus for the single particle model and the  $2 \times 2 \times 2$  particles model is shown in Fig. 17. Corresponding to the figure, we can observe that with increasing the interface thickness and the number of inclusions involved in the model would lead to increasing the effective Young’s modulus.

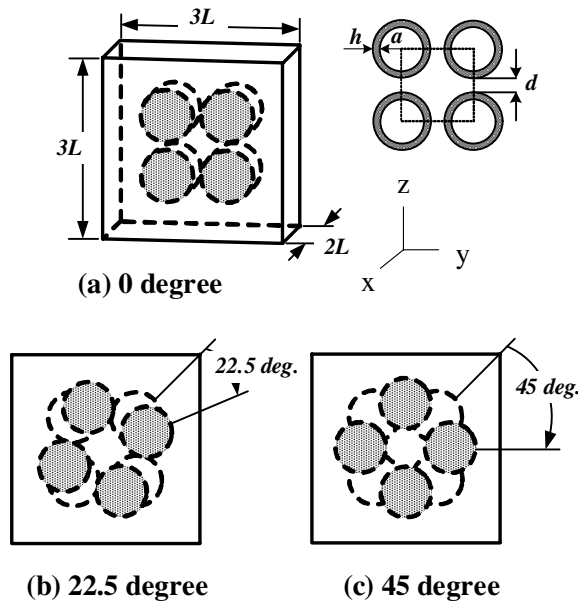
### 5.3 Influences of the orientation arrangements of the inclusions

In this section, the effects of the orientation arrangements of the inclusions on the effective Young’s modulus are investigated.

Assuming the same color spherical particles as a part, three specific difference in directional angles ( $\theta = 0^\circ, 22.5^\circ, 45^\circ$ ) between the part and the part are taken into account as Fig. 18 (a)-(c). The  $2 \times 2 \times 2$  spherical particles (inclusions) of radius  $a$ , surrounded with a thin coating (interphase) having a uniform thickness  $h$ , are embedded within the solid model (matrix) with thickness, width, and height dimensions ( $3L \times 3L \times 2L$ ). The dimensions are:  $a = 8.5 \mu m, h = 0.5 \mu m, d = 6 \mu m$  and  $L = 21.31 \mu m$ , and the material properties used for the analysis are given in Tab. 4.

**Table 4** : The properties of the constituent materials for the solid model

Constituent Materials	Young's Modulus (GPa)	Poisson's ratio
Particle (inclusion)	$E(p) = 84.0$	$\nu(p) = 0.22$
Coating (inter-phase)	$E(in) = 6.0$	$\nu(in) = 0.34$
Matrix	$E(m) = 4.0$	$\nu(m) = 0.34$

**Figure 18** : Three specific difference in directional angles between the two particle parts: (a) 0 degree (model-1); (b) 22.5 degree (model-2); (c) 45 degree (model-3)

In the HIE-FE model, only one inclusion with its HIE stiffness matrix is needed be calculated for the others. A total of  $362 \times 8$  master nodes are used to model in the HIE sub-domain. A total of 23226, 30415 and 25855 four-node tetrahedral elements are used with  $\theta = 0^\circ$ ,  $22.5^\circ$  and  $45^\circ$  in the FE sub-domain, respectively.

A comparison of the effective Young's modulus in the x-direction of the HIE-FE model with different orientation of inclusion is tabulate in Tab. 5. It can be see that model NO.1 possesses the highest effective Young's modulus of the all; in the contrarily, the lowest modulus occurs when the difference of directional angles equal to  $45^\circ$ . It is also clearly shown that the maximum difference between the highest and lowest values is estimated about 5.02%. In general, with the increase of the difference of directional angle, the effective Young's modulus may

consequently decrease. As a result, the effective Young's modulus is closely dependent on the orientation arrangements of the inclusions in these models.

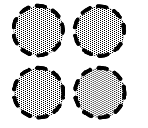
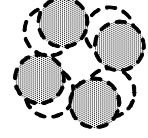
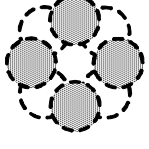
## 6 Conclusion

Complete 3-D HIE algorithms were well developed based on the similarity partition concept and particular matrix manipulations. In this work, one of the major contributions is to construct the 3-D HIE numerical procedures merged with heterogeneity effects. Another contribution is converting the "3-D HIE" into the concept of "3-D HIE". An innovative 3-D HIE-FE coupling scheme that associates with the HIE and the conventional FE through the commercial FEM software *ABAQUS* is also outlined.

The proposed method for investigating the mechanical response of heterogeneous materials with embedded inclusions was demonstrated. A special element containing an inclusion was developed to model the heterogeneity effects. The element formulations were derived using conventional FEM with similarity concept and matrix condensation operations. The resulting element stiffness matrix only involves master node degrees of freedom over the element's boundary. Because identical stiffness holds for similar isoparameter elements, only one inclusion with its HIE stiffness matrix is required to be calculated once and it is also valid for the other ones. This makes numerical evaluation of the element stiffness matrix relatively easy and efficient. This leads to significant reduction in total degrees of freedom without sacrificing accuracy in solutions. The proposed method is verified against finite element solutions. Excellent agreement is obtained and irregular stress distribution surrounding the inclusions can be accurately captured.

The proposed "3-D HIE" method was extended to model the inclusions in particulate-reinforced composites with the presence of the interphases. The HIE can be viewed as an element with boundary-only discretization. The approach provides flexibility in parametric study of the interphase, since, when the geometry, size, or material property of the interphase are changed, only a small change for the FE mesh is required. In addition, the influences of interphase thickness and material properties of inclusions on the effective Young's modulus have been investigated. Numerical results show that the thickness and material properties of the interphases can have significant effects on the mechanical behavior of the com-

**Table 5** : Three specific difference in directional angles between the two particle parts: (a) 0 degree (model-1); (b) 22.5 degree (model-2); (c) 45 degree (model-3)

2×2×2 particles model			
	Model 1	Model 2	Model 3
Inclusion Orientation			
Effective Young's modulus (GPa)	6.1963/1.0	6.0992/0.98	5.8998/0.95

posites, such as effective Young's modulus.

The numerical results showed that the effective Young's modulus also depends on the orientation arrangements of inclusions with interphases. Since only one inclusion with its HIE stiffness matrix is required for calculation once and it is also valid for the other ones, it is more easier and efficient to model 3-D composite material reinforced with arbitrarily multiple thickly coated particles (inclusions) than FEM. The corresponding CPU time and PC memory storage on these computations were also significantly reduced.

The proposed method provides another accurate and efficient numerical technique for the modeling and analysis of the inclusions in heterogeneous materials. Thermal loading in the present HIEM and extension of the 3-D model to couple with genetic algorithm to study the parametric optimization design will be interesting topics and can be carried out readily.

**Acknowledgement:** The authors would like to thank the National Science Council, Taiwan, R.O.C., for financially supporting this research under grant NSC94-2212-E-194-010 and NSC94-2212-E-194-013.

## References

**Agrwal, B. D.; Broutman, L. J.** (1974): Three-dimensional finite element analysis of spherical particle composites. *Fibre Sci Technol*, vol. 7, pp. 63-77.

**Böhm, H. J.; Han, W.; Eckschlager, A.** (2004): Multi-inclusion unit cell studies of reinforcement stresses and particle failure in discontinuously reinforced ductile matrix composite. *CMES: Computer Modeling in Engineering & Science*, vol. 5, no. 1, pp. 5-20.

**Chen, X. L.; Liu, Y. J.** (2001): Multiple-cell modeling

of fiber-reinforced composites with the presence of interphases using the boundary element method. *Comput Mater Sci*, vol. 21, pp. 86-94.

**Dong, C. Y.; Lo, S. H.; Cheung, Y. K.** (2003): Numerical solution of 3D elastostatic inclusion problems using the volume integral equation method. *Comput Methods Appl Mech Eng*, vol. 192, pp. 95-106.

**Guo, Z. H.** (1979): Similar isoparametric elements. *Sci Bull*, vol. 24, no. 13, pp. 577-582.

**Hibbitt; Karlsson; Sorensen** (2002): ABAQUS User's Manual Version 6.3-1, USA.

**Kwon, Y. W.; Bang, H.** (2000): The finite element method using MATLAB, second ed., CRC Press, New York

**Lagache, M.; Agbossou, A.; Pastor, J.; Muller, D.** (1994): Role of interphase on the elastic behavior of composite materials: theoretical and experimental analysis. *J Compos Mater*, vol. 28, pp.1140-1157.

**Liu, D. S.; Chiou, D. Y.** (2003): A coupled IEM/FEM approach for solving elastic problem with multiple cracks. *Int J Solids Struct*, vol. 40, pp. 1973-1993.

**Liu, D. S.; Chiou, D. Y.** (2003): 3D IEM formulation with an IEM/FEM coupling scheme for solving elastostatic problems. *Adv Eng Softw*, vol. 34, pp. 309-320.

**Liu, D. S.; Chiou, D. Y.** (2005): Modeling of inclusions with interphases in heterogeneous material using the infinite element method. *Comput Mater Sci*, vol. 31, pp. 405-420.

**Liu, Y. J.; Xu, N.; Luo, J. F.** (2000): Modeling of interphases in fiber-reinforced composites under transverse loading using the boundary element method. *J Appl Mech*, vol. 67, pp. 41-49.

**Luo, J. F.; Liu, Y. J.; Berger, E. J.** (1998): Analy-

sis of two-dimensional thin structures (from micro- to nano-scales) using the boundary element method. *Comput Mech*, vol. 22, pp. 404-412.

**Luo, J. F.; Liu, Y. J.; Berger, E. J.** (2000): Interfacial stress analysis for multi-coating systems using an advanced boundary element method. *Comput Mech*, vol. 24, pp. 448-455.

**Okada, H.; Fukui, Y.; Kumazawa, N.** (2004): Homogenization analysis for particulate composite materials using the boundary element method. *CMES: Computer Modeling in Engineering & Science*, vol. 5, no. 2, pp. 135-149.

**Okada, H.; Liu, C. T.; Ninomiya, T.; Fukui, Y.; Kumazawa, N.** (2004): Analysis of particulate composite materials using an element overlay technique. *CMES: Computer Modeling in Engineering & Science*, vol. 6, no. 4, pp. 333-347.

**Silvester, P.; Cermak, I. A.** (1969): Analysis of coaxial line discontinuities by boundary relaxation, *IEEE Trans Microwave Theory Tech*, vol. 17, no. 8, pp. 489-495.

**Thatcher, R. W.** (1975): Singularities in the solution of Laplace's equation in two dimensions. *J Inst Math Appl*, vol. 16, pp. 303-319.

**Thatcher, R. W.** (1978): On the finite element method for unbounded region. *SIAM J Numer Anal*, vol. 15, pp. 466-477.

**Wacker, G.; Bledzki, A. K.; Chate, A.** (1998): Effect of interphase on the transverse Young's modulus of glass/epoxy composites. *Compos Part A*, vol. 29, pp. 619-626.

**Wu, Y.; Dong, Z.** (1995): Three-dimensional finite element analysis of composites with coated spherical inclusion. *Mater Sci Eng A*, vol. 203, pp. 314-323.

**Ying, L. A.** (1995): Infinite element methods, Peking University Press and Vieweg Publishing.

**Zhang, J.; Katsube, N.** (1995): A hybrid finite element method for heterogeneous materials with randomly dispersed elastic inclusions. *Finite Elem Anal Des*, vol. 19, pp. 45-55.

**Zhang, J.; Katsube, N.** (1995): A hybrid finite element method for heterogeneous materials with randomly dispersed rigid inclusions. *Int J Numer Methods Eng*, vol. 38, pp. 1635-1653.

